NASA TECHNICAL NOTE

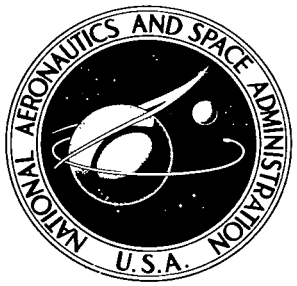

STRUCTURAL EFFICIENCIES OF FIVE COMPRESSION PANELS WITH CURVED ELEMENTS

by Gary L. Giles

Langley Research Center
Hampton, Va. 23365

NATIONAL AERONAUTICS AND SPACE ADMINISTRATION • WASHINGTON, D. C. • DECEMBER 1971

1. Report No.	2. Government Accession No.	3. Recipient's Catalog No.
NASA TN D-6479		

4. Title and Subtitle

STRUCTURAL EFFICIENCIES OF FIVE COMPRESSION PANELS WITH CURVED ELEMENTS

5. Report Date: December 1971

6. Performing Organization Code:

7. Author(s)

Gary L. Giles

8. Performing Organization Report No.: L-6546

10. Work Unit No.: 134-14-05-02

9. Performing Organization Name and Address

NASA Langley Research Center
Hampton, Va. 23365

11. Contract or Grant No.:

13. Type of Report and Period Covered: Technical Note

12. Sponsoring Agency Name and Address

National Aeronautics and Space Administration
Washington, D.C. 20546

14. Sponsoring Agency Code:

15. Supplementary Notes

16. Abstract

Structural-efficiency analyses are used to determine the minimum-mass proportions of some panel configurations loaded in uniaxial compression. Five panel constructions, four of which incorporate circular-arc elements and the other a beaded-web corrugation, are shown to have improved structural efficiencies over conventional configurations. In addition to the structural-efficiency equations, which give the mass equivalent flat-plate thickness of the panel necessary to carry a given load, related design equations for calculating the cross-sectional dimensions of these minimum-mass panels are presented. The upper and lower limits of loading, where the design constraints of minimum gage or material yield strength become the dominant design conditions, are established and the corresponding design equations which are applicable outside these limits are also presented.

17. Key Words (Suggested by Author(s))

Structural efficiency
Wide columns
Weight strength
Compression-panel design

18. Distribution Statement

Unclassified – Unlimited

19. Security Classif. (of this report)	20. Security Classif. (of this page)	21. No. of Pages	22. Price*
Unclassified	Unclassified	32	$3.00

*For sale by the National Technical Information Service, Springfield, Virginia 22151

STRUCTURAL EFFICIENCIES OF FIVE COMPRESSION PANELS WITH CURVED ELEMENTS

By Gary L. Giles
Langley Research Center

SUMMARY

Structural-efficiency analyses are used to determine the minimum-mass proportions of some panel configurations loaded in uniaxial compression. Five panel constructions, four of which incorporate circular-arc elements and the other a beaded-web corrugation, are shown to have improved structural efficiencies over conventional configurations. In addition to the structural-efficiency equations, which give the mass equivalent flat-plate thickness of the panel necessary to carry a given load, related design equations for calculating the cross-sectional dimensions of these minimum-mass panels are presented. The upper and lower limits of loading, where the design constraints of minimum gage or material yield strength become the dominant design conditions, are established and the corresponding design equations which are applicable outside these limits are also presented.

INTRODUCTION

The term "wide column" is often used to denote a compression panel of sufficiently small curvature and of sufficient width to render the buckling load independent of curvature and boundary conditions along the unloaded edges. If the bending stiffness in the axial (loading) direction is large compared to the bending stiffness in the transverse direction, rather large transverse curvatures may have little influence on the buckling load. Hence, skin panels on the upper surface of aircraft wings, the interstage and intertank structures of launch vehicles, etc., where the primary loading is axial compression, are often analyzed as wide columns.

The present paper provides the analyses of five new wide-column configurations which have improved structural efficiency over conventional configurations and can be fabricated using conventional sheet-metal forming techniques. Four of the configurations incorporate circular-arc elements (see figs. 1 and 2) and the other is a beaded-web corrugation (see fig. 3). Although these configurations do not have smooth aerodynamic surfaces, they could be used for the primary structures of hypersonic aircraft or space

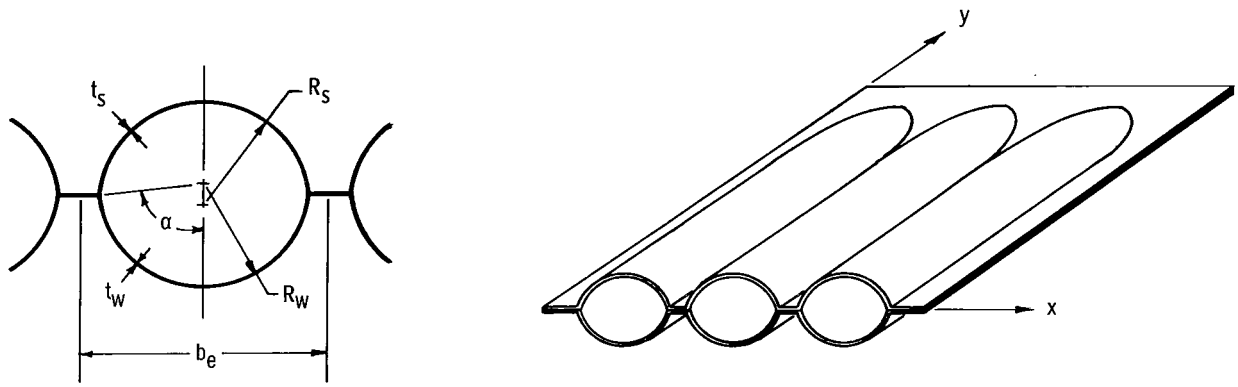

(a) Tubular.

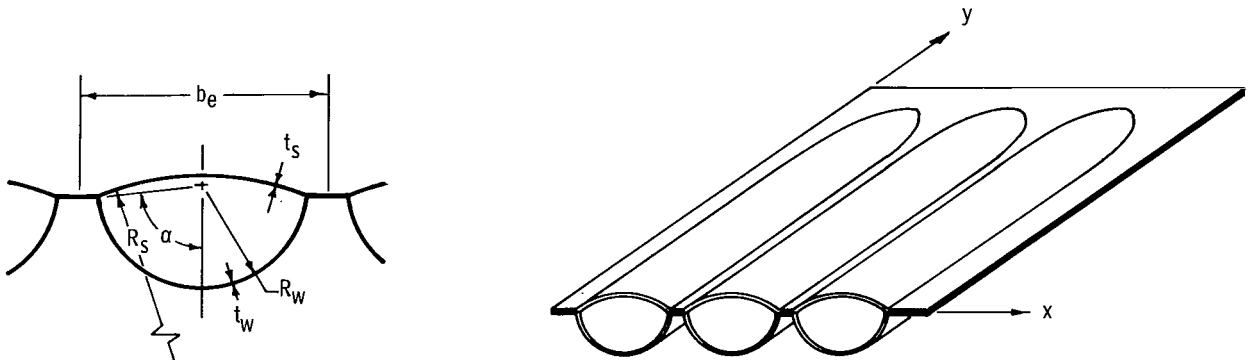

(b) Convex beaded skin.

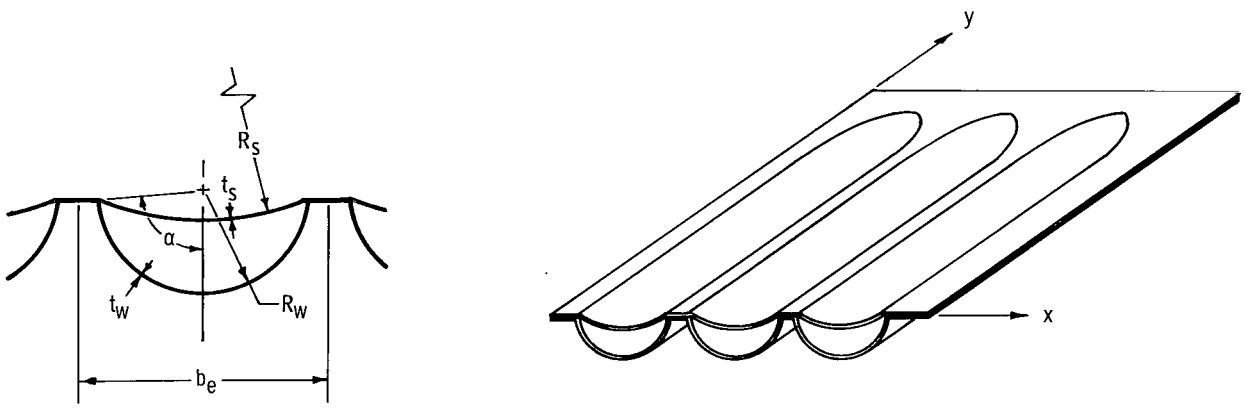

(c) Concave beaded skin.

Figure 1.- Beaded-skin wide-column configurations.

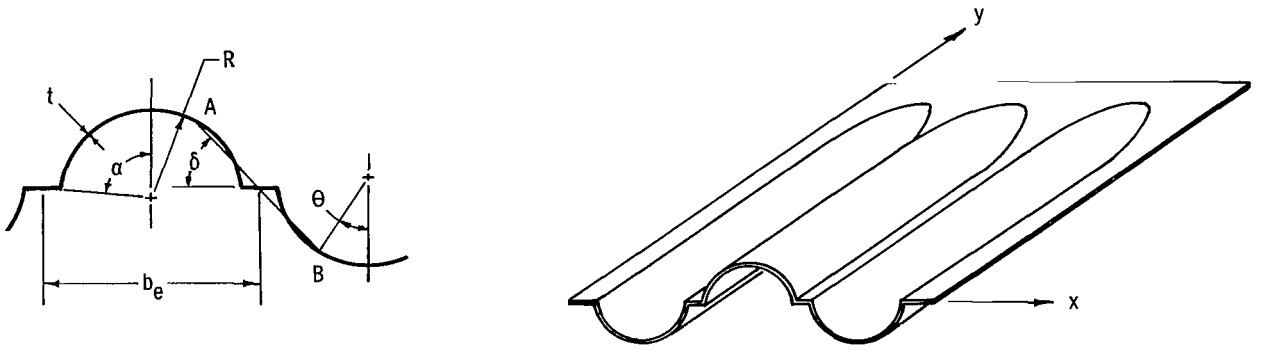

Figure 2.- Circular-arc corrugation.

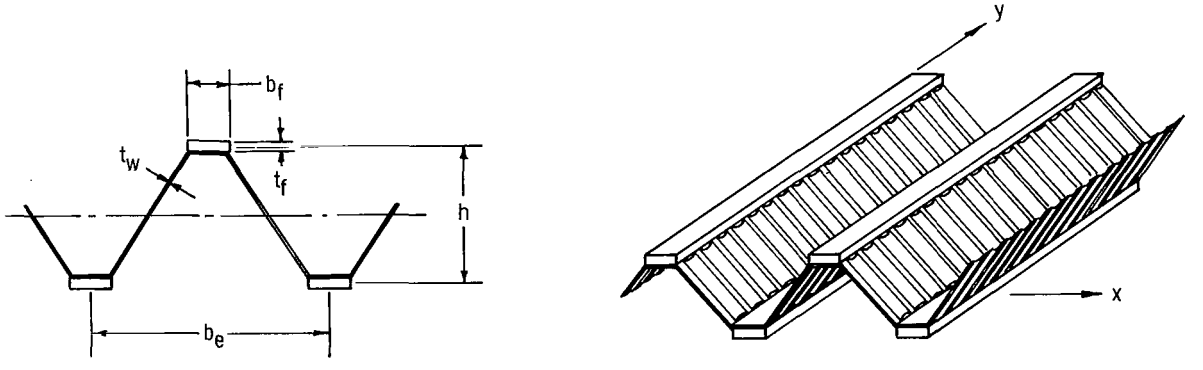

Figure 3.- Beaded-web corrugation.

shuttle vehicles in areas which require external heat shields. In addition some of the concepts have only small undulations which may be acceptable as an external surface if properly alined with the airstream. Potential uses also exist where a smooth surface is not necessary as in the interstage and intertank structures of launch vehicles. The structural efficiencies of the new concepts are compared with Z-stiffened and flat-element corrugation panels as well as honeycomb-core sandwich and waffle-grid stiffened panels under uniaxial load.

Simultaneous occurrence of local and general buckling is the criterion used in the derivation of the basic structural-efficiency equations. These equations are applicable between the limits of loading where the design constraints of minimum gage or material yield strength become the dominant design condition. The cut-off limits for minimum gage and yield strength are given along with the corresponding design equations which are applicable when these limits are exceeded.

SYMBOLS

Values are given in both SI and U.S. Customary Units. Calculations were made in the U.S. Customary Units.

b	panel width, m (in.)
b_f, b_e	width of flange and elements, respectively, m (in.)
c	exponent in structural-efficiency equation (eq. (1))
d	exponent in local-buckling equation for circular-arc element of beaded skin (eq. (A11))
E	modulus of elasticity, N/m^2 (psi)
h	total depth of beaded-web corrugation, m (in.)
H_1, H_2, H_3, H_4	geometric parameters (defined by eqs. (B5), (B6), (B7), and (B8), respectively)
I	area moment of inertia per unit width
J	torsional stiffness constant per unit width
K	buckling coefficient
k	coefficient in equation (A11)
l	panel length, m (in.)
N_x	axial compressive load per unit width, N/m (lb/in.)
Q	geometric parameter (defined in eq. (B4))
R	radius, m (in.)
r_R	ratio of radii of web and skin segments

r_t	ratio of thickness of web and skin segments
t	thickness, m (in.)
t_f	thickness of flange elements, m (in.)
$\bar{t}$	mass equivalent flat-plate thickness of a stiffened panel, m (in.)
Y	geometric parameter (defined in eq. (B11))
α	half-angle used in defining circular-arc segment, deg
δ	angle between flat and orthotropic panel in circular-arc corrugation (see fig. 2), deg
ϵ	structural efficiency factor
η	plasticity-reduction factor
$\bar{\eta}$	effective plasticity-reduction factor
θ	angle defining simple support boundary condition of orthotropic panel in circular-arc corrugation (see fig. 2), deg
$\xi_1, \xi_2, \xi_3, \xi_4, \bar{\xi}$	geometric parameters (defined by eqs. (A2), (A4), (A5), (A7), and (A13) or (A14), respectively)
ρ_c	core density, kg/m^3 (lb/in^3)
ρ_f	density of direct-load-carrying material, kg/m^3 (lb/in^3)
σ	stress, N/m^2 (psi)
σ_{cy}	compressive yield stress, N/m^2 (psi)

Subscripts:

a	applied loading

g	general or overall buckling
l	local buckling
min	minimum
s	skin
w	web
x	refers to x-direction
y	refers to y-direction

STRUCTURAL-EFFICIENCY EQUATION

For a wide column of a given length and carrying a given inplane compressive loading, structural-efficiency analysis can be used to determine the geometric proportions which yield minimum structural mass. The established principle for obtaining optimum proportions is to design for simultaneous occurrence of the local and general modes of buckling under the applied loading (refs. 1 to 4). When the equations describing the above conditions are combined in an efficiency analysis, the following general form of structural-efficiency equation is obtained as discussed in reference 2:

$$\text{Loading-material index} = \text{Efficiency factor} \times (\text{Mass index})^{c}$$

For wide columns the expression is

$$\frac{N_x}{l\bar{\eta}E} = \epsilon\left(\frac{\bar{t}}{l}\right)^{c} \tag{1}$$

The loading-material index is specified by the design requirements for a panel of length l, constructed of a material having a modulus of elasticity E and an effective plasticity-reduction factor $\bar{\eta}$ based on local and general buckling, and having the compressive end loading N_x. The mass of the required panel is obtained from the corresponding mass index $\bar{t}/l$. The exponent c is a characteristic of each configuration and results from equating the local and general buckling stresses of the panels. For a particular column configuration the structural efficiency factor ϵ is dependent on the geometric proportions and is maximized to obtain maximum structural efficiency or minimum mass.

High structural efficiency results when the loading parameter $N_x/l\bar{\eta}E$ is maximum for a given thickness parameter $\bar{t}/l$ or when $\bar{t}/l$ is minimum at a constant value of $N_x/l\bar{\eta}E$. Conventionally, the results are presented on log-log graphs of the mass index $\bar{t}/l$ versus the loading-material index $N_x/l\bar{\eta}E$. The equations plot as straight lines with $1/c$ specifying the slope and $(1/\epsilon)^{1/c}$ locating the ordinate for a given abscissa. Structural-efficiency curves of this type provide a convenient means of comparing candidate structural configurations, and related design equations can be used to determine the detailed cross-sectional geometry of the optimized panels.

Results from the efficiency analyses of the new panel configurations considered in this paper are presented in the following sections. The efficiency equations along with the related design equations are derived in the appendixes. The appendixes give the buckling equations used for each configuration and an explanation of the method used to combine these equations to obtain the form of the structural-efficiency equation.

RESULTS AND DISCUSSIONS

Wide-Column Configurations and Efficiency Factors

Beaded-skin construction.- Three beaded-skin configurations which are fabricated by forming circular-arc beads in two sheets and welding them together at the flats are shown in figure 1. The high local-buckling stress of the circular-arc elements makes possible the efficient use of materials in all three of these configurations. The tubular panel is the most efficient of these configurations because of its higher column-buckling strength. Increasing the radius of the arcs for the outer skin, as in the convex and concave beaded-skin panels, provides a smoother outer surface. However, the decrease in overall column-buckling strength results in some decrease in structural efficiency.

These beaded-skin configurations have similar geometric properties, and a structural-efficiency analysis which applies to all three configurations is contained in appendix A. The resulting structural-efficiency factor is given by equation (A17). Numerical results which were calculated from this equation for a range of geometric parameters are presented in figures 4 to 6. The radius of the skin is set relative to the radius of the web at the ratio $R_S/R_W = 2$ for the convex and concave beaded-skin panels. Structural efficiencies of the beaded-skin configurations are shown to be strongly dependent on the arc of the web α and relatively insensitive to changes in the width of the flats expressed by the parameter b_e/R_W.

Practical fabrication techniques limit the maximum structural efficiency of these configurations. The highest efficiencies are obtained when the arc of the web is equal to or greater than 90^o. However, forming such angles between the flat and the arc may be

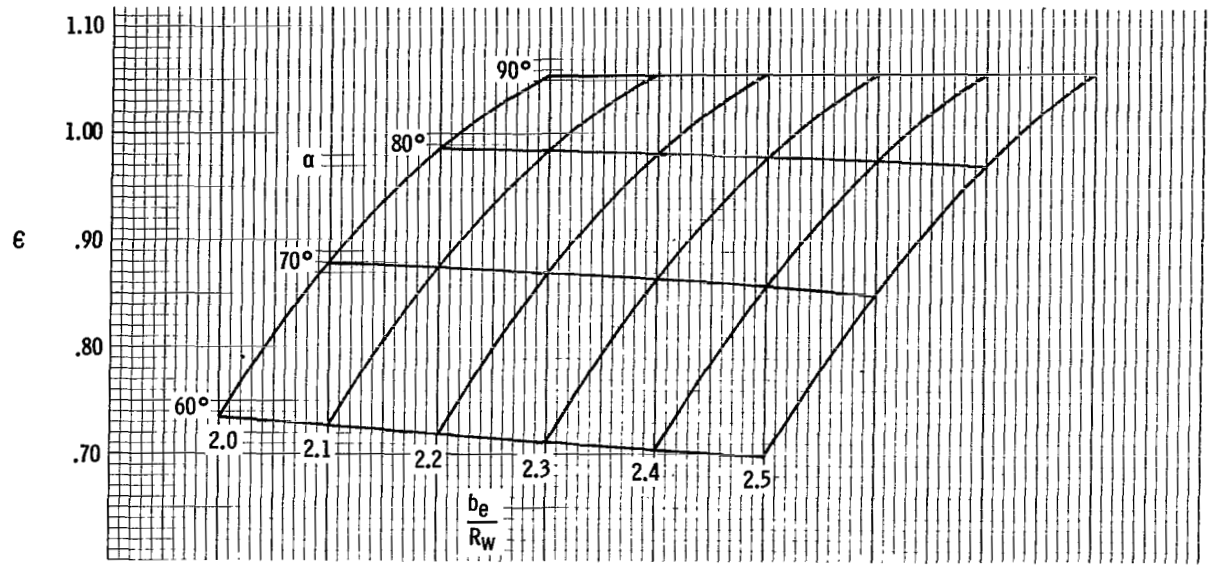

Figure 4.- Structural-efficiency factor for tubular panels $\left(\frac{R_s}{R_w} = \frac{t_s}{t_w} = 1.0\right)$.

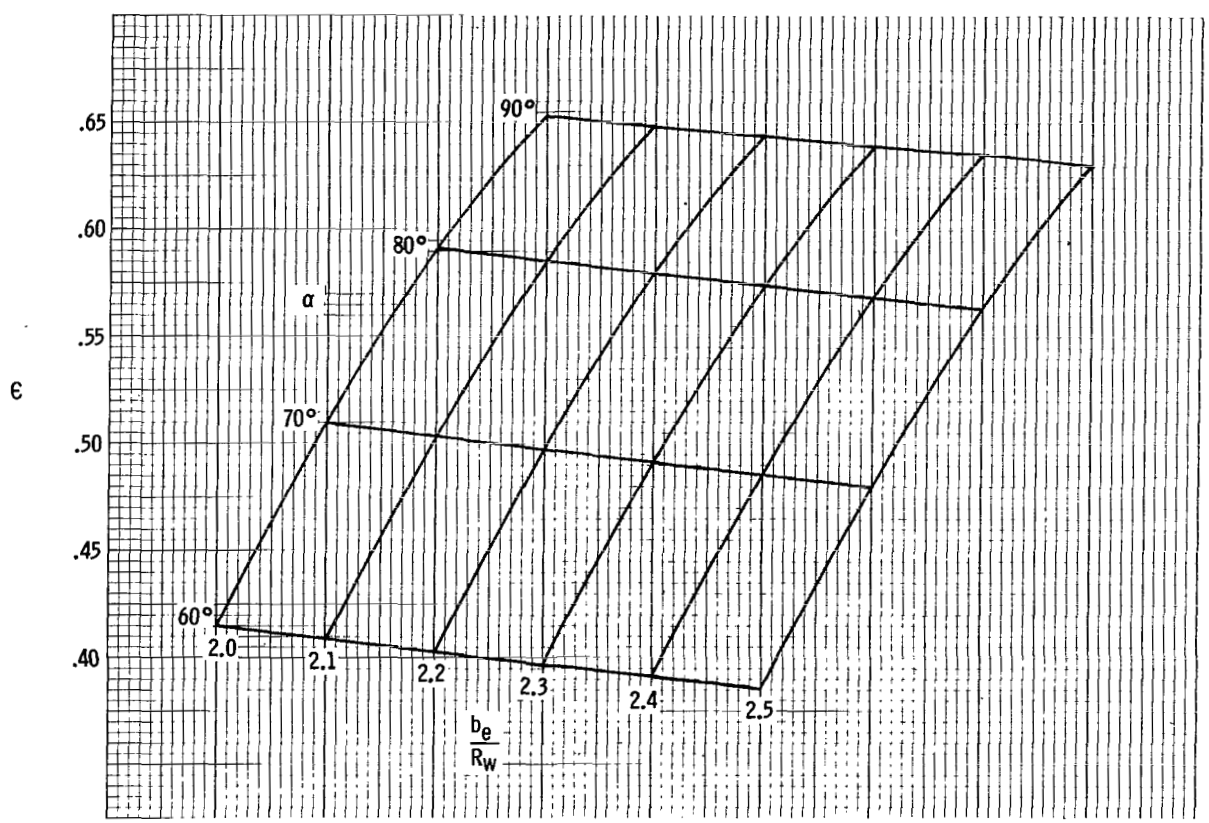

Figure 5.- Structural-efficiency factor for convex beaded-skin panels $\left(\frac{R_s}{R_w} = \frac{t_s}{t_w} = 2.0\right)$.

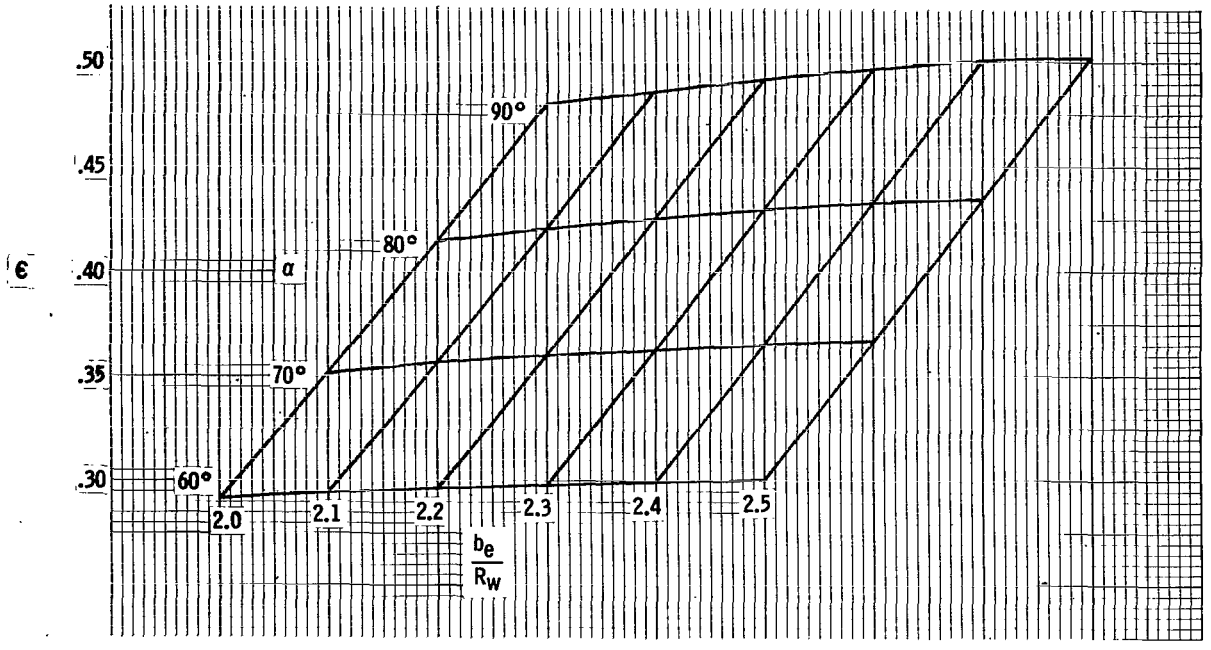

Figure 6.- Structural-efficiency factor for concave beaded-skin panels $\left(\frac{R_s}{R_w} = \frac{t_s}{t_w} = 2.0\right)$.

impractical, and a lesser angle might be required with corresponding reduction in efficiency. The width of the flats provided for welding can be selected to facilitate fabrication without significantly influencing the efficiency factor.

Since these configurations contain closed sections, they have some twisting stiffness. To include the beneficial effect of this torsional stiffness and the edge restraint at the unloaded edges, the equation for buckling of a simply supported orthotropic plate is used for general buckling. A plate width b must be specified for this calculation. Square panels where $b = l$ were selected for the results presented in this paper. The efficiency factors for square panels including this torsional stiffness are given in the analysis in appendix A.

Circular-arc corrugation.- The circular-arc corrugation which is formed from a single sheet is shown in figure 2. This configuration, like the beaded-skin configurations, incorporates circular arcs because of their high local-buckling strength. The flat segments may be necessary in practical aircraft construction to attach clips for supporting heat shields and for splicing panel segments. When the circular-arc corrugation was initially considered in this study, it was thought that the flat segments would prevent local buckling in the section between crests of adjacent arcs (section A-B of fig. 2). However, in a subsequent test of a circular-arc corrugation incorporating a flat segment (ref. 5), local buckling did in fact occur in this section. The behavior appeared to be local buckling

of an orthotropic plate with edge supports along the crests of adjacent arcs. The orthotropic-plate buckling of this section is considered to be the local buckling of the cross section in the present paper and is used for the structural-efficiency analysis given in appendix B. This assumed local-buckling behavior, which is based on limited experimentation, is highly simplified and additional tests are needed to establish firmly the local-buckling stress for different geometric proportions of this particular cross section.

The calculated efficiency factor of the circular-arc corrugation is given in figure 7 for different geometric proportions of the cross section. These results show that the efficiency of the configuration increases as the width of the flat segment decreases. Thus the flat segment actually decreases the efficiency of the circular-arc corrugation.

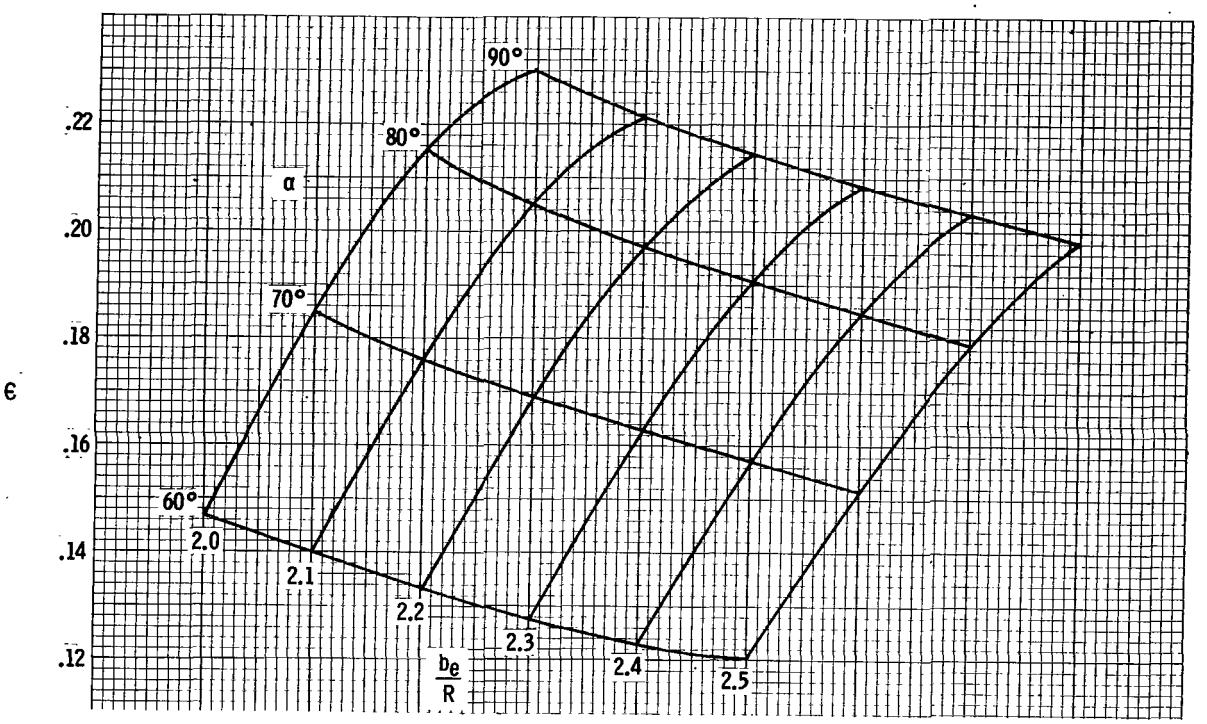

Figure 7.- Structural-efficiency factor for circular-arc corrugation.

Beaded-web corrugation.- The beaded-web corrugation is composed of cap strips connected by a beaded core as shown in figure 3. This configuration gains its efficiency by having the direct-load-carrying material concentrated in the cap strips at the extreme fibers of the cross section. These cap strips are proportioned to prevent local buckling, and they provide a high bending stiffness for a low overall panel mass. Shear forces between the cap strips are transmitted by the beaded web; however, this web does not carry any longitudinal compression. As the behavior of an idealized model is used in this analysis, no investigation was made of the adequacy of the web for stabilizing the cap

strips. Tests of panels are needed to determine the actual buckling behavior of this configuration. Although the present analysis is restricted to an idealized model, the assumptions made are such that the results should indicate the potential efficiency of the configuration and provide initial guidelines for designing beaded-web-corrugation panels.

An analogy can be established between the beaded-web corrugation and a honeycomb-core sandwich panel. The cap strips correspond to the skin sheets and the beaded web corresponds to the core material. The efficiency factor determined in appendix C for both of these configurations is $\epsilon = \frac{K\pi^2}{27\left(\rho_c/\rho_f\right)^2}$. For square simply supported honeycomb-core sandwich panels $K = 4.0$, and for beaded-web wide columns $K = 1.0$. The ratio of the core or beaded-web mass to the skin or cap-strip mass will be referred to as core density. Higher structural efficiency is achieved with lower core densities. To provide increased efficiency over the honeycomb-core sandwich, which has a practical lower core density of 0.02, the beaded-web corrugation must have a core density of less than 0.01. The core of honeycomb sandwich is made up of cells which are formed from many sheets of foil-gage material. However, the core material of the beaded-web corrugation is concentrated into a single sheet and low core densities can be used without going below the practical minimum gage thickness. The web minimum gage is dependent on the material used, but for many materials a core density of less than 0.01 can be used for the beaded-web corrugation.

Comparison of Structural Efficiencies

Design equations for the five wide-column configurations are presented in tables 1 to 3, which include structural-efficiency equations for the values of panel loading where buckling is the dominant design condition. To be useful for practical design throughout the range of loading, the design constraints of material yield strength for high loading and minimum gage for low loading must also be considered. The cut-off load limits where material yield strength or minimum gage become the dominant design condition are established in the appendixes, and corresponding design equations which are applicable outside these limits are given in the tables. The structural efficiencies of the configurations will be compared for each of these load ranges.

Designs based on buckling.- The structural-efficiency curves for the five wide-column configurations based on simultaneous occurrence of buckling modes are presented in figure 8. The curves for the tubular, convex and concave beaded skin where $R_S/R_W = 2$, and circular-arc-corrugation configurations are for panels with semicircular

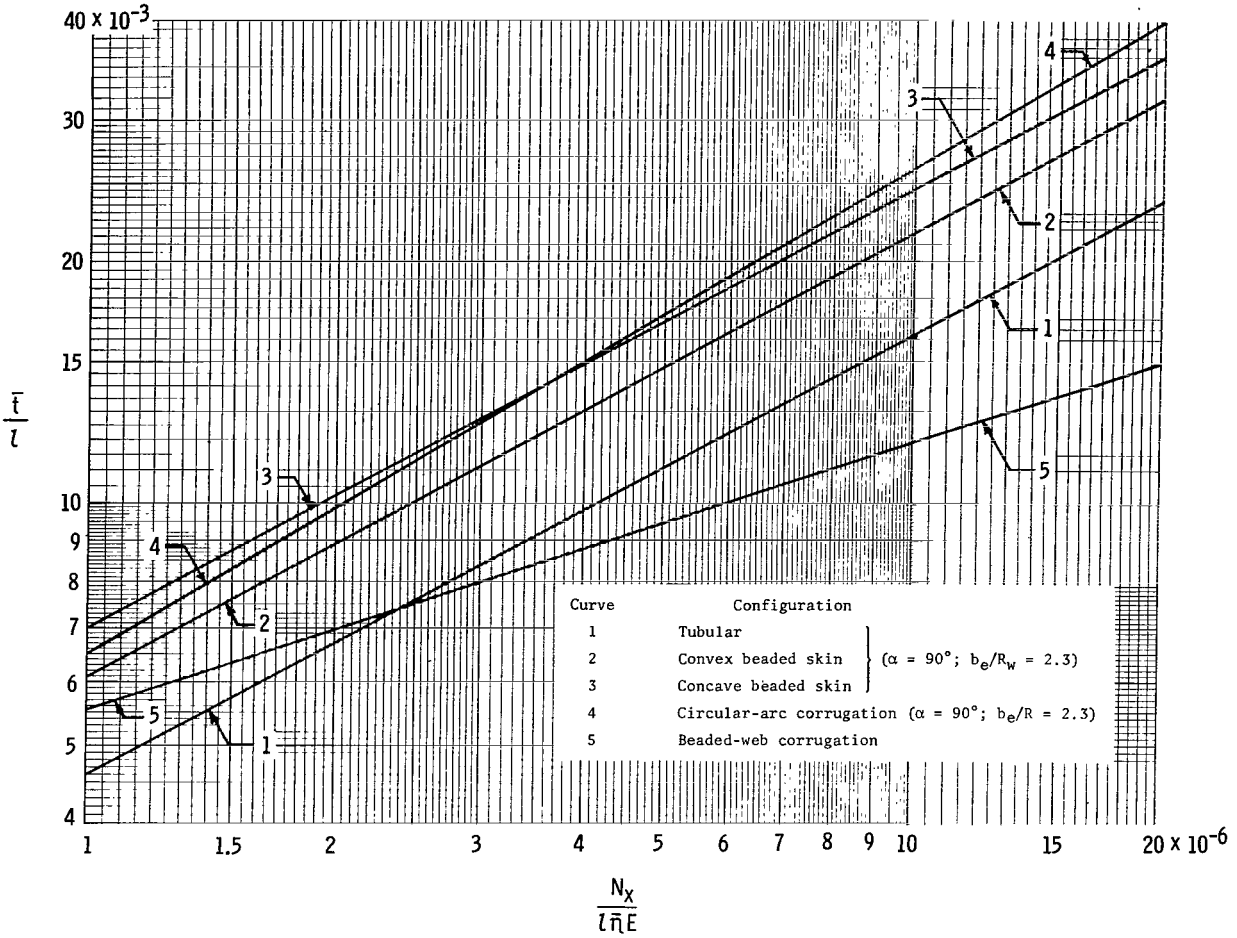

Figure 8.- Structural-efficiency comparison of the five test columns. (Designs based only on buckling.)

arcs ($\alpha = 90^{o}$) and flats 0.3 times the radius of the arcs. A value of core density of 0.008 is used for the efficiency curve for the beaded-web corrugation.

All the curves for the beaded-skin configurations have the same slope with the tubular panel being the most efficient. Increasing the radius of the arcs of the outer skin, as in the convex- and concave-beaded-skin configurations, provides a smoother outer surface. However, the decrease in overall column-buckling strength results in the corresponding decrease in structural efficiency. The curves for the convex and concave beaded skin and circular-arc corrugation are in a narrow band on the structural-efficiency plot. Because the curve for the circular-arc corrugation has a greater slope than those for the beaded skin, higher structural efficiency is provided by the circular-arc corrugation at low loading, but it becomes less efficient at high loading. The beaded-web corrugation is shown to be the most efficient concept except at low values of loading.

The five new configurations are compared with some conventional panel concepts in figure 9. The Z-stiffened and flat-element-corrugation wide columns and honeycomb-core sandwich and waffle-grid stiffened plates were selected for comparison of structural efficiencies. The plate configurations, which have high bending stiffness in both the axial and transverse directions, are compared with the wide columns to determine their relative efficiencies for carrying uniaxial loads. Because the honeycomb and waffle-plate configurations have a characteristic dimension of panel width b rather than panel length l, the same principles are used as for the beaded-skin panels with closed sections, where square plates ($b = l$) were used to compare plate configurations with wide columns.

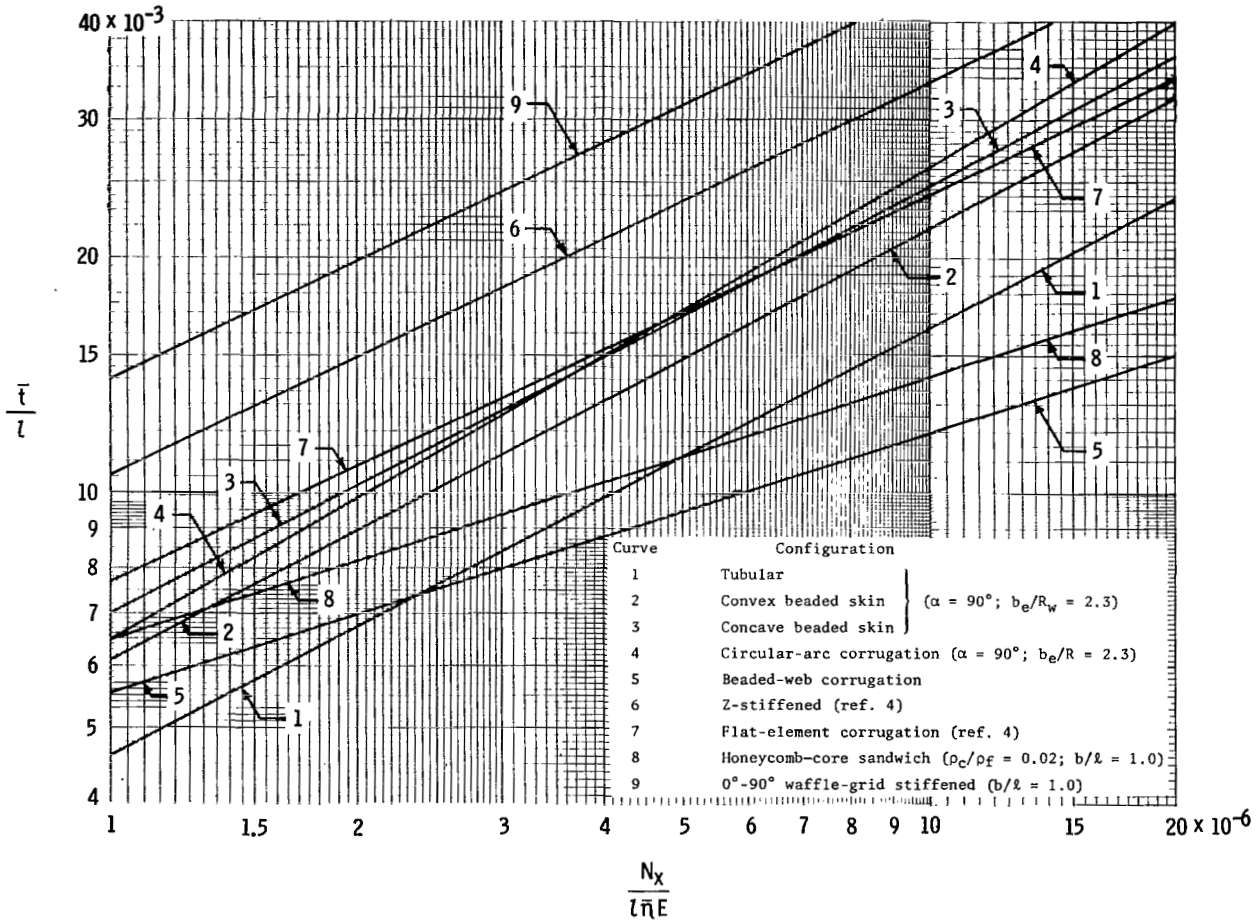

Figure 9.- Structural-efficiency comparison of several wide-column configurations. (Designs based only on buckling.)

All five new configurations are shown to be more efficient than the Z-stiffened wide columns. The flat-element corrugation is in the same band on the efficiency plot as the convex- and concave-beaded-skin and circular-arc corrugations. Relatively higher

structural efficiency is provided by the flat-element corrugation at lower loading, but it becomes relatively less efficient for high loading. The curve for the honeycomb-core sandwich has the same slope as the curve for the beaded-web corrugation, but because of the higher core density that is required for the honeycomb it has a relatively lower structural efficiency. The curve for the waffle-grid stiffened panel is the uppermost curve on the structural efficiency plot and hence is shown to be a relatively inefficient configuration for carrying uniaxial load. A general comparison of all the efficiency curves on figure 9 shows that the five new configurations can provide improved structural efficiency over conventional concepts, and these configurations could have potential use in design applications where low structural mass is important.

Yield-strength and minimum-gage considerations.- The effects of including the practical design constraints of material yield strength and minimum gage in the analysis of the five new panel configurations are shown by the structural-efficiency curves of figure 10. Although the range of loading where buckling governs the design (middle segments of the curves) is limited by the design constraints, this range is still quite large for the less efficient configurations. With increasing efficiency of configurations the range of loading where buckling governs is decreased.

For increasing values of loading the stress in the cross section of a panel is increased until the material yield strength is reached. Above this load the cross-sectional area of the panel must be increased to prevent the applied stress from exceeding the material yield strength. This constraint is presented in figure 10 as a material-yield-strength parameter. The value of $\sigma_{cy}/E = 0.0078$ corresponds to the material properties of a titanium alloy; $\sigma_{cy} = 827.3$ MN/m^2 (12×10^4 psi) and $E = 106.2$ GN/m^2 (15.4×10^6 psi). All of the material included in the mass equivalent flat-plate thickness $\bar{t}$ of the beaded-skin and circular-arc-corrugation constructions carries direct load and can be stressed up to the material yield strength. The efficiency curves for these configurations plot as straight lines until they intersect and follow the line of the material yield strength. Only the cap strips of the beaded-web corrugation carry direct load. The core material, which does not carry any direct load but is included in the mass equivalent thickness, makes this configuration relatively less efficient in the high loading range. Unlike the other configurations, the resulting efficiency curve for the beaded-web corrugation plots as a curved line for designs governed by yield strength, and because of the core mass the curve does not intersect the line of the material yield strength.

For decreasing values of loading the sheet thicknesses in the column cross sections decrease until the minimum gage limit is reached. To show the comparative effects on the structural-efficiency graph a value of minimum web gage of $t_w = 0.254$ mm (0.010 in.) was selected for the beaded-skin and the circular-arc-corrugation configurations. This value was nondimensionalized by a panel length of 1.016 m (40.0 in.) for the results

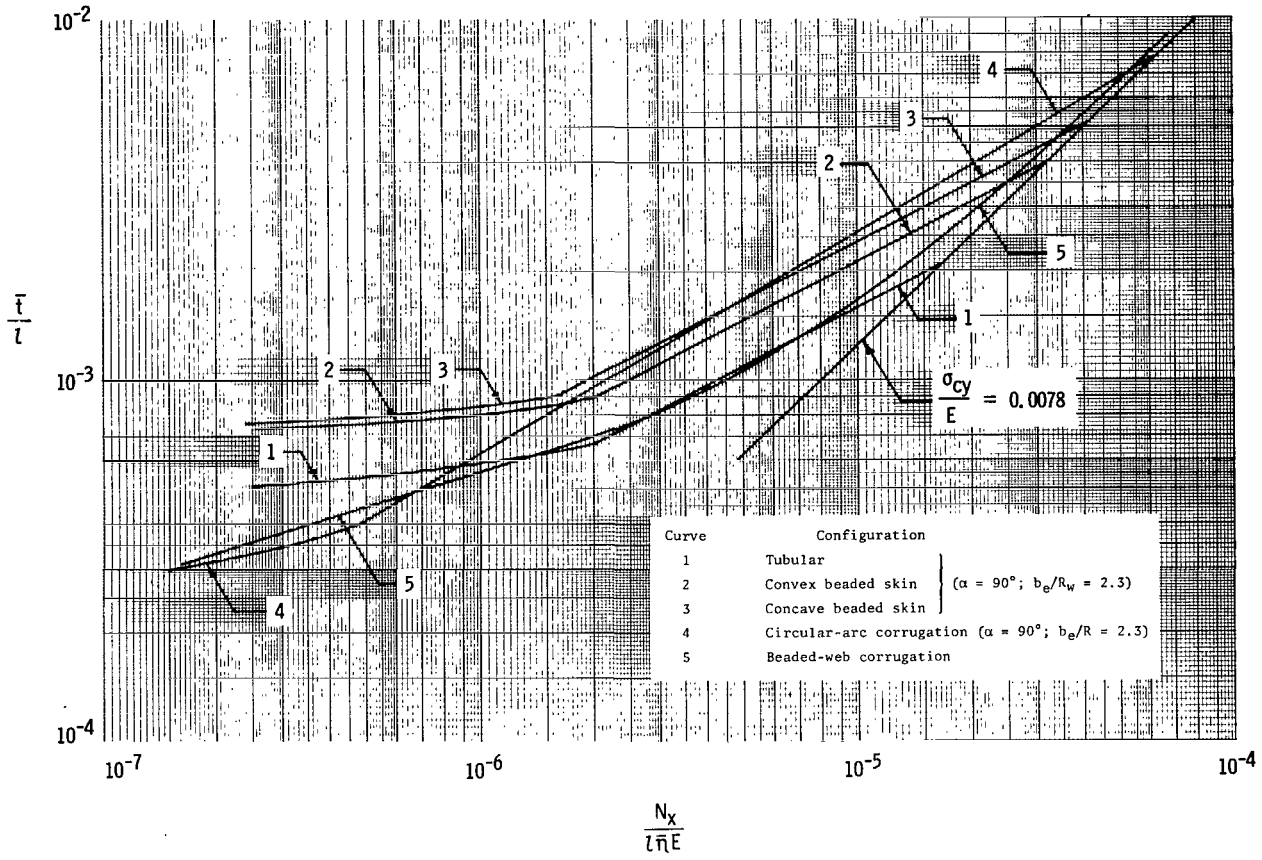

Figure 10.- Structural-efficiency comparison of five wide-column configurations considering minimum gage, buckling, and yield strength.

presented in figure 10. In the region of loading where buckling governs the design the half-angle of the web was fixed ($\alpha = 90^{o}$ for the results shown). Below the minimum gage limit t_w is fixed and α is allowed to decrease. The values of α which will provide a cross section of sufficient depth to prevent general column buckling are determined in this region of loading. The relative efficiencies of the beaded-skin configurations are approximately the same in both the region where buckling governs the design and the region where minimum gage governs. However, for loadings less than the minimum-gage limit the circular-arc corrugation becomes more efficient than the beaded-skin configurations since it is formed from one rather than two minimum-gage sheets.

Below the minimum-gage limit for the beaded-web corrugation the thickness of the web sheet was fixed and the depth h which gave a minimum-mass panel was determined. The results shown in figure 10 are for a minimum web gage of $t_w = 0.127$ mm (0.005 in.) nondimensionalized by a panel length of $l = 1.016$ m (40.0 in.). For this example the

slope of the curve segment for the panels governed by minimum gage does not differ appreciably from the slope of the segment where panel buckling governs the design.

CONCLUDING REMARKS

Structural-efficiency analyses are used to determine the minimum-mass proportions of five panel configurations. These panel constructions, four of which incorporate circular-arc elements and the other a beaded-web corrugation, are shown to have improved structural efficiencies over conventional configurations. High local-buckling strength of the curved sections gives high structural efficiency for the panels incorporating circular-arc elements. Efficient design is obtained with the beaded-web corrugation because the compressive load-carrying material is positioned at its extreme fibers and very low core densities are attainable without use of foil-gage material.

In addition to the structural-efficiency equations, which give the mass equivalent flat-plate thickness of the panel necessary to carry a given load, related design equations for calculating the cross-sectional dimensions of these minimum-mass panels are presented. These structural-efficiency equations and related design equations are applicable only for the range of loading where buckling governs the design. The upper and lower limits of loading, where the other design constraints of minimum gage or material yield become the dominant design conditions, are established. The corresponding design equations which are applicable outside these limits are presented, thus, providing design equations for the complete load range.

Langley Research Center,
National Aeronautics and Space Administration,
Hampton, Va., October 29, 1971.

APPENDIX A

BEADED-SKIN CONSTRUCTION

In this appendix the structural-efficiency analysis of the three structural elements having closed sections shown in figure 1 is presented.

Geometric Properties

Mass equivalent thickness:

$$\bar{t} = t_w \frac{R_w}{b_e} \xi_1 \tag{A1}$$

where

$$\xi_1 = 2\alpha + \frac{2}{r_R r_t} \sin^{-1}\left(r_R \sin\alpha\right) + \left(\frac{b_e}{R_w} - 2\sin\alpha\right)\left(\frac{1}{r_t} + 1\right) \tag{A2}$$

$$r_R = \frac{R_w}{R_s}$$

$$r_t = \frac{t_w}{t_s}$$

Area moment of inertia of cross section about its centroid:

$$I_x = t_w R_w^2 \frac{R_w}{b_e}\left(\xi_3 - \frac{\xi_2^2}{\xi_1}\right) \tag{A3}$$

where

$$\xi_2 = 2(\sin\alpha - \alpha\cos\alpha) + (-1)^N\left(\frac{2}{r_t r_R^2}\right)\left[r_R \sin\alpha - \sqrt{1 - \left(r_R \sin\alpha\right)^2}\,\sin^{-1}\left(r_R \sin\alpha\right)\right] \tag{A4}$$

(For tubular and convex beaded skin $N = 1$ and for concave beaded skin $N = 2$.)

$$\xi_3 = \alpha - 3\sin\alpha\cos\alpha + 2\alpha\cos^2\alpha + \frac{1}{r_R^3 r_t}\left[\left(3 - 2r_R^2\sin^2\alpha\right)\sin^{-1}\left(r_R\sin\alpha\right) - 3r_R\sin\alpha\sqrt{1 - \left(r_R\sin\alpha\right)^2}\right] \tag{A5}$$

Torsional stiffness of one bay of cross section:

$$J_x = t_w R_w^2 \left(\frac{R_w}{b_e}\right) \xi_4 \tag{A6}$$

where

$$\xi_4 = \frac{2\left[\alpha - \sin\alpha\cos\alpha + (-1)^N \frac{1}{r_R^2} \sin^{-1}\left(r_R \sin\alpha\right) - (-1)^N \sqrt{\frac{1}{r_R^2} - \sin^2\alpha}\right]^2}{\alpha + \frac{r_t}{r_R} \sin^{-1}\left(r_R \sin\alpha\right)} \tag{A7}$$

(For tubular and convex beaded skin $N = 1$ and for concave beaded skin $N = 2$.)

Applied Stress

The equation for applied stress is

$$\sigma_a = \frac{N_x}{\bar{t}} = \frac{N_x}{t_w} \frac{b_e}{R_w} \frac{1}{\xi_1} \tag{A8}$$

Buckling Modes

For general buckling considering the panel to be a wide column:

$$\sigma_g = \frac{\pi^2 \eta_g E I_x}{\bar{t} l^2} \tag{A9}$$

To include the beneficial effect of torsional stiffness and the edge restraint at the unloaded edges, the equation for buckling of a simply supported orthotropic plate is used. This buckling equation is usually written in terms of the plate width b. A comparison with wide-column results can be made for square panels where $b = l$. The equation for general buckling, when the flexural rigidity in the transverse direction is much less than in the axial direction and Poisson's ratio (μ) in the transverse direction is considered to be zero (ref. 6), can be written as

$$\sigma_g = \frac{\pi^2 \eta_g E}{\bar{t} l^2}\left[I_x + \frac{J_x}{2(1+\mu)}\right] \tag{A10}$$

Equation (A9) differs from (A10) by the torsional stiffness term $J_x/2(1+\mu)$.

The form of the equation for local buckling of the circular-arc elements is taken to be:

$$\sigma_l = k\eta_l E\left(\frac{t}{R}\right)^d \tag{A11}$$

where k and d are constants which depend on the value of t/R. A curve of equation (A11) is fitted to the recommended design curve given in reference 7 for buckling of cylinders in axial compression, and a comparison of these curves is shown in figure 11. For the range $2 \times 10^{-3} \leqq t/R \leqq 1.5 \times 10^{-2}$ good agreement is obtained with the recommended curve when $k = 1.75$ and $d = 1.35$. The use of the cylinder-buckling data for the buckling stress of circular-arc elements is shown to be slightly conservative in reference 8.

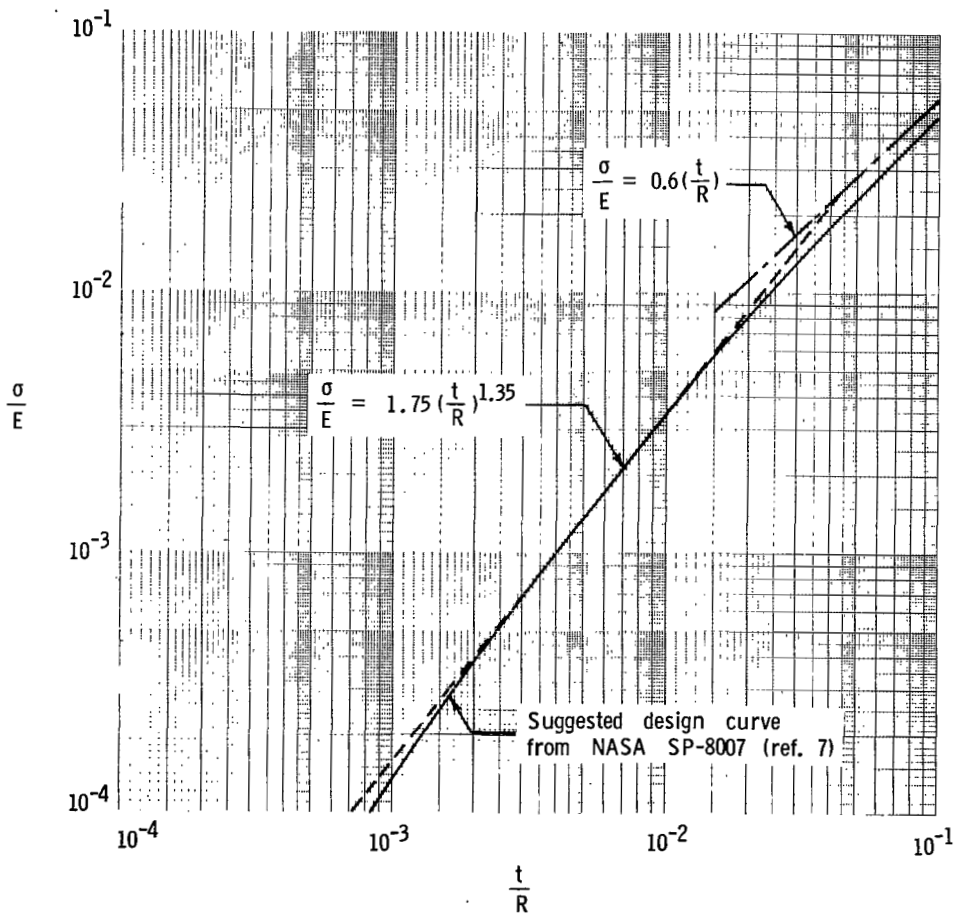

Figure 11.- Buckling stress for isotropic cylinders subjected to axial compression.

Structural-Efficiency Equation for Designs Governed by Buckling

For minimum-mass design the condition used is that $\sigma_a = \sigma_g = \sigma_l$. Equations (A8), (A9) or (A10), and (A11) are now combined to give the following equation:

$$\sigma_a^{2}\sigma_g\sigma_l^{\frac{2}{d}} = \sigma_a^{3+\frac{2}{d}} = \pi^2 k^{\frac{2}{d}} \bar{\xi} \left(\frac{b_e}{R_w}\right)^2 \eta_l^{\frac{2}{d}} \eta_g E^{\frac{2}{d}+1} \left(\frac{N_x}{l}\right)^2 \tag{A12}$$

where

$$\bar{\xi} = \frac{\xi_1\xi_3 - \xi_2^{2}}{\xi_1^{4}} \tag{A13}$$

when the panel is assumed to act as a wide column and

$$\bar{\xi} = \frac{\xi_1\xi_3 - \xi_2^{2}}{\xi_1^{4}} + \frac{\xi_4}{2(1+\mu)\xi_1^{3}} \tag{A14}$$

when the torsional stiffness is included in the analysis for a square panel. Combination of equations (A8) and (A12) yields the efficiency equation:

$$\frac{N_x}{l\bar{\eta}E} = \epsilon \left(\frac{\bar{t}}{l}\right)^{\frac{3d+2}{d+2}} \tag{A15}$$

where

$$\bar{\eta} = \eta_l^{\frac{2}{d}} \eta_g \tag{A16}$$

$$\epsilon = \left[\pi^2 k^{\frac{2}{d}} \left(\frac{b_e}{R_w}\right)^2 \bar{\xi}\right]^{\frac{d}{d+2}} \tag{A17}$$

A local-buckling coefficient which includes the interaction of the buckling of the individual portions of the cross sections is not available for the configurations considered. Therefore, the conservative assumption is made that the individual arc portions have pin joints along their boundaries. The local-buckling stresses are equated for the arc portions of the skin and web, yielding $r_t = r_R$ $\left(t_w/t_s = R_w/R_s\right)$. If the geometric ratios r_R and

b_e/R_w are specified, the resulting panel efficiency can be determined. The corresponding design equations which are applicable for the range of loading when the design is governed by buckling are given in table 1.

Design Equations for Designs Governed by Minimum Gage or Material Yield Strength

For design loadings where the design is governed by either minimum gage or material yield strength, the mass equivalent thickness necessary to meet these constraints is established directly by

$$\frac{\bar{t}}{l} = \frac{t_{w_{min}}}{l} \frac{R_w}{b_e} \xi_1 \tag{A18}$$

or

$$\frac{\bar{t}}{l} = \frac{N_x/l\bar{\eta}E}{\sigma_{cy}/\bar{\eta}E} \tag{A19}$$

The cut-off limits for the range of loading where the structural-efficiency equation (A15) is applicable are established by substituting equations (A18) and (A19) into (A15). Outside these limits the mass equivalent thickness is greater than that required for buckling. Above the cut-off limit of loading for material yield strength the mass equivalent thickness which gives a stress in the column cross section equal to the material yield strength is determined. Below the cut-off limit for minimum gage the sheet thickness of the web is fixed at the minimum-gage value, and the depth of cross section is reduced by decreasing the half-angle of the web α. This reduction in the depth of the cross section gives a lower mass equivalent thickness $\bar{t}$. The cut-off limits and corresponding design equations are given in table 1.

APPENDIX B

CIRCULAR-ARC CORRUGATION

The circular-arc corrugation shown in figure 2 is analyzed as a wide column since the transverse bending stiffness and the torsional stiffness are negligible.

Geometric Properties

Mass equivalent thickness:

$$\bar{t} = t\frac{R}{b_e}\left(2\alpha - 2\sin\alpha + \frac{b_e}{R}\right) \tag{B1}$$

Area moment of inertia per unit width of cross section about the x-axis shown in figure 2:

$$I_x = tR^2\frac{R}{b_e}(\alpha - 3\sin\alpha\cos\alpha + 2\alpha\cos^2\alpha) \tag{B2}$$

Area moment of inertia per unit width of local segment between points A and B about an axis through A and B:

$$(I_x)_{AB} = tR^2Q \tag{B3}$$

where

$$Q = \frac{2(H_1 - H_2 + H_3) + H_4}{2\left[(\cos\theta - \cos\alpha)^2 + \left(\frac{b_e}{2R} - \sin\theta\right)^2\right]^{1/2}} \tag{B4}$$

$$H_1 = \frac{1}{2}(\alpha - \theta) - \frac{1}{4}\sin 2\left(\delta + \frac{\pi}{2} - \theta\right) + \frac{1}{4}\sin 2\left(\delta + \frac{\pi}{2} - \alpha\right) \tag{B5}$$

$$H_2 = \frac{\left[\cos\left(\delta + \frac{\pi}{2} - \alpha\right) - \cos\left(\delta + \frac{\pi}{2} - \theta\right)\right]^2}{\alpha - \theta} \tag{B6}$$

$$H_3 = (\alpha - \theta)\left[\sin\left(\theta + \frac{\pi}{2} - \delta\right) - \frac{\cos\left(\delta + \frac{\pi}{2} - \alpha\right) - \cos\left(\delta + \frac{\pi}{2} - \theta\right)}{\alpha - \theta}\right]^2 \tag{B7}$$

$$H_4 = \frac{1}{12}\left(\frac{b_e}{R} - 2 \sin \alpha\right)^3 \sin^2\delta \tag{B8}$$

$$\tan \delta = \frac{\cos \theta - \cos \alpha}{\frac{b_e}{2R} - \sin \theta} \tag{B9}$$

Transverse moment of inertia of local segment based on developed length between points A and B:

$$\left(I_y\right)_{AB} = t^3 Y \tag{B10}$$

where

$$Y = \frac{\frac{1}{12}\left[(\cos \theta - \cos \alpha)^2 + \left(\frac{b_e}{2R} - \sin \theta\right)^2\right]^{1/2}}{\alpha - \theta + \frac{b_e}{2R} - \sin \alpha} \tag{B11}$$

Applied Stress

The equation for applied stress is:

$$\sigma_a = \frac{N_x}{\bar{t}} \tag{B12}$$

Buckling Modes

General buckling of wide column using the Euler equation:

$$\sigma_g = \pi^2 \eta_g E\left(\frac{R}{l}\right)^2\left(\frac{\alpha - 3 \sin \alpha \cos \alpha + 2\alpha \cos^2\alpha}{2\alpha - 2 \sin \alpha + \frac{b_e}{R}}\right) \tag{B13}$$

Local buckling is considered to occur as orthotropic-panel buckling of the section between points A and B. The buckling equation (ref. 6) can be written as:

$$\sigma_l = \frac{2\pi^2 \eta_l E}{b_{eff}^2 t_{eff}} \sqrt{(I_x)_{AB}(I_y)_{AB}} \tag{B14}$$

where b_{eff} is the width and t_{eff} is the cross-sectional area of the orthotropic panel between points A and B. In the present analysis it is assumed that this panel is simply supported at points A and B. The location of these points of simple support is specified by the angle θ, which is treated as a variable in this analysis. Geometric parameters α and b_e/R are selected, and then the value of θ which gives the minimum local-buckling load is determined. This method gives conservative results. Actual panel tests are required to determine more precisely the effective width of this orthotropic panel, hence the value of θ.

Structural-Efficiency Equation for Designs Governed by Buckling

The criterion used for minimum-mass design is that $\sigma_a = \sigma_g = \sigma_l$. These stresses given in equations (B12), (B13), and (B14) are combined as follows:

$$\sigma_a^2 \sigma_g \sigma_l^2 = \sigma_a^5 = \eta_g \eta_l^2 E^3 \left(\frac{N_x}{l}\right)^2 \frac{\pi^6}{4} \frac{(\alpha - 3 \sin\alpha \cos\alpha + 2\alpha \cos^2\alpha) QY}{\left(\frac{R}{b_e}\right)^2 \left(2\alpha - 2\sin\alpha + \frac{b_e}{R}\right)^3 \left\{\left[(\cos\theta - \cos\alpha)^2 + \left(\frac{b_e}{2R} - \sin\theta\right)^2\right]\left(\alpha - \theta + \frac{b_e}{2R} - \sin\alpha\right)^2\right\}} \tag{B15}$$

Substitution of $\sigma_a = \frac{N_x}{\bar{t}}$ into equation (B15) yields the efficiency equation

$$\frac{N_x}{l\bar{\eta}E} = \epsilon \left(\frac{\bar{t}}{l}\right)^{\frac{5}{3}} \tag{B16}$$

where

$$\bar{\eta} = \left(\eta_g \eta_l^2\right)^{\frac{1}{3}} \tag{B17}$$

$$\epsilon = \left\{ \frac{\pi^6}{4} \left[\frac{(\alpha + \sin\alpha\cos\alpha - 2\alpha\cos^2\alpha)QY}{(\cos\theta - \cos\alpha)^2 + \left(\frac{b_e}{2R} - \sin\theta\right)^2 \left(\frac{R}{b_e}\right)^2 \left(\alpha - \theta + \frac{b_e}{2R} - \sin\alpha\right)^2} \right] \right\}^{\frac{1}{3}} \tag{B18}$$

Curves for this efficiency factor are given in figure 7 for the geometric proportions of $60^o \leqq \alpha \leqq 90^o$ and $2.0 \leqq b_e/R \leqq 2.5$. These data were calculated by holding α and b_e/R at constant values and varying the angle θ until the lowest value of the efficiency factor ϵ was determined. The value of θ changes from one set of geometric proportions to another. The method used to determine the value of θ is a conservative approximation and actual panel tests are needed to establish firmly the local-buckling behavior of this configuration. The case where $\alpha = 90^o$ and $b_e/R = 2.3$ was selected for the efficiency comparison given in figures 8 and 9.

Design Equations for Designs Governed by Minimum Gage or Material Yield Strength

The procedure used to establish the cut-off limits of loading where minimum gage or material yield strength governs the design is the same as that used in appendix A for the beaded-skin constructions. These cut-off limits and design equations which are applicable in the different regions of loading are presented in table 2.

APPENDIX C

BEADED-WEB CORRUGATION

The beaded-web corrugation shown in figure 3 has its direct-load-carrying material in its extreme fibers in order to achieve a high bending stiffness in the axial direction. This material is contained in the cap strips which are proportioned so that they will not buckle locally if their edges are simply supported. As the behavior of an idealized model of the panel was used in this analysis, no investigation was made of the adequacy of the web for stabilizing the cap strips. It was assumed that the beaded web had sufficient stiffness to provide simple support boundary conditions for the cap strips, but tests of panels are needed to determine the actual buckling behavior of this configuration. The buckling of this configuration as a wide column is the only mode of failure considered. The effect of transverse shear deformation is neglected in this analysis.

Geometric Properties

Mass equivalent thickness:

$$\bar{t} = 2\frac{b_f}{b_e}t_f + 2t_w\left[\sqrt{\left(\frac{1}{2} - \frac{b_f}{b_e}\right)^2 + \left(\frac{h}{b_e}\right)^2} + \frac{b_f}{b_e}\right] \tag{C1}$$

In this analysis the mass of the web material which carries no direct load will be given in terms of a core density. The mass of the cross section for a width b_e can be written as

$$\bar{t}\,b_e\rho_f = 2b_f t_f \rho_f + hb_e\rho_c \tag{C2}$$

or

$$\bar{t} = 2\frac{b_f}{b_e}t_f + h\frac{\rho_c}{\rho_f} \tag{C3}$$

Comparison of equations (C1) and (C3) gives a core density of

$$\frac{\rho_c}{\rho_f} = 2\frac{t_w}{h}\left[\sqrt{\left(\frac{1}{2} - \frac{b_f}{b_e}\right)^2 + \left(\frac{h}{b_e}\right)^2} + \frac{b_f}{b_e}\right] \tag{C4}$$

Area moment of inertia per unit width of cross section:

$$I_x = \frac{b_f}{b_e}\frac{t_f h^2}{2} \tag{C5}$$

Buckling Mode

General buckling:

$$N_x = \frac{K\pi^2 \eta_g E I_x}{l^2} = K\pi^2 \eta_g E \frac{b_f}{b_e}\frac{t_f h^2}{2l^2} \tag{C6}$$

Structural-Efficiency Equation for Designs Based on Buckling

Equation (C3) can be written as

$$\frac{\bar{t}}{l} = \frac{h}{l}\left(2\frac{b_f}{b_e}\frac{t_f}{h} + \frac{\rho_c}{\rho_f}\right) \tag{C7}$$

Solving for h/l from equation (C7) and substituting into equation (C6) gives the efficiency equation

$$\frac{N_x}{l\bar{\eta}E} = \epsilon\left(\frac{\bar{t}}{l}\right)^3 \tag{C8}$$

where

$$\epsilon = \frac{K\frac{\pi^2}{2}\frac{b_f}{b_e}\frac{t_f}{h}}{\left(2\frac{b_f}{b_e}\frac{t_f}{h} + \frac{\rho_c}{\rho_f}\right)^3} \tag{C9}$$

Optimum structural efficiency occurs when

$$\frac{b_f t_f}{b_e h} = \frac{1}{4}\frac{\rho_c}{\rho_f} \tag{C10}$$

and

$$\epsilon = \frac{K\pi^2}{27\left(\frac{\rho_c}{\rho_f}\right)^2} \tag{C11}$$

For the beaded-web corrugation which buckles as a wide column the buckling coefficient K equals 1.0. Equations (C3) and (C6) which will be combined to give a structural-efficiency equation are the same for a square honeycomb-core sandwich panel if $b_f/b_e = 1.0$ and $K = 4.0$.

Design Equations for Designs Governed by Minimum Gage or Material Yield Strength

The cut-off limits where minimum gage or material yield strength governs the design along with corresponding sets of design equations to cover the entire range of loading are presented in table 3. Above the cut-off limit for material yield strength the areas of the cap strips, which will give a stress under the applied load equal to the material yield stress, are determined. The corresponding depth of the beaded-web corrugation h is governed by general buckling. Below the minimum-gage cut-off limit the thickness of the beaded web is fixed at the minimum value. The depth of the cross section h is then reduced to give the minimum-mass configuration which will carry the applied load. The ratio b_f/b_e which determines the width of the cap strips can be arbitrarily selected for the beaded-web corrugation. However, the proportions of the resulting cap strips must be such that local buckling of these strips does not occur.

REFERENCES

1. Shanley, F. R.: Weight-Strength Analysis of Aircraft Structures. McGraw-Hill Book Co., Inc., 1952.

2. Crawford, Robert F.; and Burns, A. Bruce: Strength, Efficiency, and Design Data for Beryllium Structures. ASD Tech. Rep. 61-692, U.S. Air Force, 1962.

3. Gerard, George: Optimum Structural Design Concepts for Aerospace Vehicles: Bibliography and Assessment. AFFDL-TR-65-9, U.S. Air Force, June 1965. (Available from DDC as AD 468 335.)

4. Emero, Donald H.; and Spunt, Leonard: Wing Box Optimization Under Combined Shear and Bending. J. Aircraft, vol. 3, no. 2, Mar.-Apr. 1966, pp. 130-141.

5. Plank, P. P.; Sakata, I. F.; Davis, G. W.; and Richie, C. C.: Hypersonic Cruise Vehicle Wing Structure Evaluation. NASA CR-1568, 1970.

6. Timoshenko, Stephen P.; and Gere, James M.: Theory of Elastic Stability. Second ed., McGraw-Hill Book Co., Inc., 1961, pp. 403-404.

7. Anon.: Buckling of Thin-Walled Circular Cylinders. NASA SP-8007, 1965. (Revised 1968.)

8. Gerard, George; and Becker, Herbert: Handbook of Structural Stability. Pt. III – Buckling of Curved Plates and Shells. NACA TN 3783, 1957.

TABLE 1.- DESIGN EQUATIONS FOR BEADED-SKIN CONSTRUCTIONS

Design governed by buckling	Design governed by minimum gage	Design governed by material yield strength
Structural-efficiency equation:	Lower cut-off limit for structural-efficiency equation:	Upper cut-off limit for structural-efficiency equation:
$\frac{N_x}{l\bar{\eta}E} = \epsilon\left(\frac{\bar{t}}{l}\right)^{\frac{3d+2}{d+2}}$	$\frac{N_x}{l\bar{\eta}E} = \epsilon\left(\frac{t_{w_{min}}}{l}\frac{R_w}{b_e}\xi_1\right)^{\frac{3d+2}{d+2}}$	$\frac{N_x}{l\bar{\eta}E} = \left[\epsilon\left(\frac{\bar{\eta}E}{\sigma_{cy}}\right)^{\frac{3d+2}{d+2}}\right]^{\frac{-2d}{d+2}}$
where		
$\epsilon = \left[\pi^2 k^{\frac{2}{d}}\left(\frac{b_e}{R_w}\right)^2\frac{\left(\xi_1\xi_3 - \xi_2^2\right)}{\xi_1^4}\right]^{\frac{d}{d+2}}$		
Corresponding design equations:	Design equations applicable below limit:	Design equations applicable above limit:
$\bar{t} = l\left(\frac{N_x}{\epsilon l\bar{\eta}E}\right)^{\frac{d+2}{3d+2}}$	$\bar{t} = l\left(\frac{t_{w_{min}}}{l}\right)\frac{R_w}{b_e}\xi_1$	$\bar{t} = l\left(\frac{N_x}{l\bar{\eta}E}\right)\left(\frac{\bar{\eta}E}{\sigma_{cy}}\right) = \frac{N_x}{\sigma_{cy}}$
$t_w = \bar{t}\left(\frac{b_e}{R_w}\right)\frac{1}{\xi_1}$	$t_w = t_{w_{min}}$	$t_w = \bar{t}\left(\frac{b_e}{R_w}\right)\frac{1}{\xi_1}$
$t_s = \frac{t_w}{r_t}$	$t_s = \frac{t_w}{r_t}$	$t_s = \frac{t_w}{r_t}$
$R_w = t_w\left(\frac{k\eta_l E\bar{t}}{N_x}\right)^{\frac{1}{d}}$		$R_w = \left(\frac{\frac{\eta_l}{\eta_g}kt_w d_l^2}{\pi^2\frac{\xi_1\xi_3 - \xi_2^2}{\xi_1^2}}\right)^{\frac{1}{2+d}}$
$R_s = \frac{R_w}{r_R}$		$R_s = \frac{R_w}{r_R}$
$b_e = \left(\frac{b_e}{R_w}\right)R_w$		$b_e = \left(\frac{b_e}{R_w}\right)R_w$

TABLE 2.- DESIGN EQUATIONS FOR THE CIRCULAR-ARC CORRUGATION

Design governed by buckling	Design governed by minimum gage	Design governed by material yield strength
Structural efficiency equation:	Lower cut-off limit for structural efficiency equation:	Upper cut-off limit for structural efficiency equation:
$\frac{N_x}{l\bar{\eta}E} = \epsilon\left(\frac{\bar{t}}{l}\right)^{\frac{5}{3}}$	$\frac{N_x}{l\bar{\eta}E} = \epsilon\left[\frac{t_{min}}{l}\frac{R}{b_e}\left(2\alpha - 2\sin\alpha + \frac{b_e}{R}\right)\right]^{\frac{5}{3}}$	$\frac{N_x}{l\bar{\eta}E} = \left[\epsilon\left(\frac{\bar{\eta}E}{\sigma_{cy}}\right)^{\frac{5}{3}}\right]^{-\frac{2}{3}}$
where ϵ is obtained from fig. 4, or eq. (B18) can be used if θ is available from test data		
Corresponding design equations:	Design equations applicable below limit:	Design equations applicable above limit:
$\bar{t} = l\left(\frac{N_x}{\epsilon l\bar{\eta}E}\right)^{\frac{3}{5}}$	$\bar{t} = l\left(\frac{t_{min}}{l}\right)\frac{R}{b_e}\left(2\alpha - 2\sin\alpha + \frac{b_e}{R}\right)$	$\bar{t} = l\left(\frac{N_x}{l\bar{\eta}E}\right)\frac{\bar{\eta}E}{\sigma_{cy}} = \frac{N_x}{\sigma_{cy}}$
$t = \frac{\bar{t}}{\frac{R}{b_e}\left(2\alpha - 2\sin\alpha + \frac{b_e}{R}\right)}$	$t = l\left(\frac{t_{min}}{l}\right)$	$t = \bar{t}\,\frac{b_e}{R}\left(\frac{1}{2\alpha - 2\sin\alpha + \frac{b_e}{R}}\right)$
$R = \left[\frac{N_x l^2}{\bar{t}\,\pi^2\eta_g E}\left(\frac{2\alpha - 2\sin\alpha + \frac{b_e}{R}}{\alpha - 3\sin\alpha\cos\alpha + 2\alpha\cos^2\alpha}\right)\right]^{\frac{1}{2}}$	$R = \left\{\frac{\eta l}{\eta_g}\frac{tl^2}{2}\frac{\sqrt{Q}\sqrt{Y}\left(2\alpha - 2\sin\alpha + \frac{b_e}{R}\right)}{\left[(\cos\theta - \cos\alpha)^2 + \left(\frac{b_e}{2R} - \sin\theta\right)^2\right]^{\frac{1}{2}}\left(\alpha - \theta + \frac{b_e}{2R} - \sin\alpha\right)(\alpha - 3\sin\alpha\cos\alpha + 2\alpha\cos^2\alpha)}\right\}^{\frac{1}{3}}$	
$b_e = \left(\frac{b_e}{R}\right)R$	$b_e = \left(\frac{b_e}{R}\right)R$	

TABLE 3.- DESIGN EQUATIONS FOR THE BEADED-WEB CORRUGATION

Design governed by buckling	Design governed by minimum gage	Design governed by material yield strength
Structural-efficiency equation:	Lower cut-off limit for structural-efficiency equation:	Upper cut-off limit for structural-efficiency equation:
$\frac{N_x}{l\bar{\eta}E} = \epsilon\left(\frac{\bar{t}}{l}\right)^3$	$\frac{N_x}{l\bar{\eta}E} = \epsilon\left\{3\,\frac{t_{w_{min}}}{l}\left[\sqrt{\left(\frac{1}{2}-\frac{b_f}{b_e}\right)^2+\left(\frac{h}{b_e}\right)^2}+\frac{b_f}{b_e}\right]\right\}^3$	$\frac{N_x}{l\bar{\eta}E} = \frac{\sigma_{cy}}{\bar{\eta}E}\left(\frac{\bar{t}}{l}-\frac{2}{\pi}\frac{\rho_c}{\rho_f}\sqrt{\frac{\sigma_{cy}}{\bar{\eta}E}}\right)$
where		where
$\epsilon = \frac{K\pi^2}{27\left(\frac{\rho_c}{\rho_f}\right)^2}$		$\frac{\bar{t}}{l} = \left(\frac{N_x}{\epsilon l\bar{\eta}E}\right)^{\frac{1}{3}}$
Corresponding design equations:	Design equations applicable below limit:	Design equations applicable above limit:
$\bar{t} = l\left(\frac{N_x}{\epsilon l\bar{\eta}E}\right)^{\frac{1}{3}}$	$t_w = l\left(\frac{t_{w_{min}}}{l}\right)$	$\bar{t} = l\left[\frac{N_x}{l\bar{\eta}E}\left(\frac{\bar{\eta}E}{\sigma_{cy}}\right)+\frac{2}{\pi}\frac{\rho_c}{\rho_f}\sqrt{\frac{\sigma_{cy}}{\bar{\eta}E}}\right]$
$h = \frac{2\bar{t}}{3\,\frac{\rho_c}{\rho_f}}$	Select $\frac{b_f}{b_e}$ and $\frac{h}{b_e}$	$h = \frac{2l}{\pi}\sqrt{\frac{\sigma_{cy}}{\bar{\eta}E}}$
Select $\frac{b_f}{b_e}$ and $\frac{h}{b_e}$	$h = \frac{2t_w}{\rho_c/\rho_f}\left[\sqrt{\left(\frac{1}{2}-\frac{b_f}{b_e}\right)^2+\left(\frac{h}{b_e}\right)^2}+\frac{b_f}{b_e}\right]$	Select $\frac{b_f}{b_e}$ and $\frac{h}{b_e}$
$t_f = \frac{\bar{t}}{6}\frac{b_e}{b_f}$	$\bar{t} = l\,\frac{4}{\pi^2}\frac{N_x}{l\bar{\eta}E}\frac{l}{h^2}+h\frac{\rho_c}{\rho_f}$	$t_f = \frac{N_x}{2\sigma_{cy}\frac{b_f}{b_e}}$
$t_w = \frac{\bar{t}}{3\left[\sqrt{\left(\frac{1}{2}-\frac{b_f}{b_e}\right)^2+\left(\frac{h}{b_e}\right)^2}+\frac{b_f}{b_e}\right]}$	$t_f = \frac{1}{2\,\frac{b_f}{b_e}}\left(\bar{t}-h\frac{\rho_c}{\rho_f}\right)$	$t_w = \frac{\frac{h}{2}\frac{\rho_c}{\rho_f}}{\sqrt{\left(\frac{1}{2}-\frac{b_f}{b_e}\right)^2+\left(\frac{h}{b_e}\right)^2}+\frac{b_f}{b_e}}$

004 001 C1 U 32 711203 S00903DS
DEPT OF THE AIR FORCE
AF WEAPONS LAB (AFSC)
TECH LIBRARY/WLOL/
ATTN: E LOU BOWMAN, CHIEF
KIRTLAND AFB NM 87117

"The aeronautical and space activities of the United States shall be conducted so as to contribute . . . to the expansion of human knowledge of phenomena in the atmosphere and space. The Administration shall provide for the widest practicable and appropriate dissemination of information concerning its activities and the results thereof."

—NATIONAL AERONAUTICS AND SPACE ACT OF 1958

NASA SCIENTIFIC AND TECHNICAL PUBLICATIONS

TECHNICAL REPORTS: Scientific and technical information considered important, complete, and a lasting contribution to existing knowledge.

TECHNICAL NOTES: Information less broad in scope but nevertheless of importance as a contribution to existing knowledge.

TECHNICAL MEMORANDUMS: Information receiving limited distribution because of preliminary data, security classification, or other reasons.

CONTRACTOR REPORTS: Scientific and technical information generated under a NASA contract or grant and considered an important contribution to existing knowledge.

TECHNICAL TRANSLATIONS: Information published in a foreign language considered to merit NASA distribution in English.

SPECIAL PUBLICATIONS: Information derived from or of value to NASA activities. Publications include conference proceedings, monographs, data compilations, handbooks, sourcebooks, and special bibliographies.

TECHNOLOGY UTILIZATION PUBLICATIONS: Information on technology used by NASA that may be of particular interest in commercial and other non-aerospace applications. Publications include Tech Briefs, Technology Utilization Reports and Technology Surveys.

Details on the availability of these publications may be obtained from:

SCIENTIFIC AND TECHNICAL INFORMATION OFFICE

NATIONAL AERONAUTICS AND SPACE ADMINISTRATION

Washington, D.C. 20546